Design of Machines and Structures, Vol. 13, No. 1 (2023), pp. 64–72.
https://doi.org/10.32972/dms.2023.006

PREDICTION OF STRAIN DISTRIBUTION DURING THE PLANE STRAIN TENSILE TEST BASED ON ARTIFICIAL NEURAL NETWORKS

RAID FEKHREDDINE MEKNASSI[1] – GÁBOR BÉRES[2] – ZSOLT LUKÁCS[3]

[1]*University of Miskolc, Department of Mechanical Technologies,*
3515 Miskolc-Egyetemváros,
metraid@uni-miskolc.hu
[2]*John von Neumann University, GAMF Faculty of Engineering and Computer Science,*
6000 Kecskemét, Izsáki út 10
beres.gabor@gamf.uni-neumann.hu
[3]*University of Miskolc, Department of Mechanical Technologies,*
3515 Miskolc, Miskolc-Egyetemváros,
zsolt.lukacs@uni-miskolc.hu
[2]*https://orcid.org/0000-0002-1496-5618*, [3]*https://orcid.org/0000-0002-6517-8382*

Abstract: In this study, finite element method was used to study the effects of various notch geometries on the strain field distributions during the plane strain tensile test for cold-rolled steel (DC01). The artificial neural network approach (ANN) and the response surface methodology (RSM) were adopted to develop the mathematical prediction models applied in the optimization procedure. The strain state was expressed by self-defined metrics, namely, the Plane Strain State Index (PSSI) and the Homogeneity Index (HI) were predicted by changing the notch angle (X degree), notch width (d mm), and notch length (c mm). The Quadratic mathematical models obtained by the RSM, and ANN presented the evolution of PSSI, and HI based on (X, d, and c). The results show that the ANN method provides more precise results compared to those of the RSM approach.

Keywords: *FEM, ANN, RSM, Tensile test, Plan strain*

1. INTRODUCTION

Predicting the formability and safety limit of material in sheet metal forming operations depends on accurate knowledge of forming behaviour under various strain states. The forming limit diagram (FLD) developed by Keeler (Keeler & Backofen, 1964) and Goodwin (Goodwin & Gorton, 1968) is a beneficial graphical tool for predicting the plastic behaviour of sheet metal, used in FEM analysis and quality optimization during production. Usually, the FLD can be determined by the Nakajima and Marciniak stretch-forming test according to the ISO 12004-2:2008 standard (Marciniak & Kuczyński, 1967), (International Organization for Standardization, 2008). The strain domain must be covered from equibiaxial tension ($\varepsilon 1 = \varepsilon 2$) to pure shear ($\varepsilon 1 = -\varepsilon 2$). Also, it is necessary to deform the specimen along a linear strain path during the different loading patterns. However, the strain path is a broken line in the actual industry. Because, unlike the laboratory simulation, there

are complex tool geometries and multi-stage forming operations for industrial sheet metal forming processes that require several passes, which means that the deformation patterns change from one pass to another.

A pre-strained plane specimen with tensile test could be an interesting alternative to determine and predict forming limit curves with non-linear path. Many authors intensively used plane strain tensile test specimens for various mechanical characterizations (Flores et al., 2010), (Kuwabara, 2007), (An, Vegter & Elliott, 2004). In our study, we intended to predict and optimize a sample geometry for the plane strain tensile test that could allow us to apply further deformation tests, which eventually leads to determining the forming limits on non-linear strain paths. Several sample geometries were investigated through simulation on ABAQUS to study and measure the different strain behaviour during the test. Firstly, we investigate the evolution of the plane strain distribution, which is characterized by the self-defined change of the plane strain state index (PSSI) and homogeneity index (HI) as a function of the specimen notch parameters: notch angle (X degree), notch width (d mm), notch length (c mm). Secondly, modelling the specimen notch parameters using the response surface methodology (RSM) and the artificial neural network (ANN) methods is carried out. Finally, the predictive capabilities of the ANN and RSM models were further compared in terms of their mean square error (RMSE), and coefficient of determination (R2).

2. MATERIAL AND SAMPLE GEOMETRY

In the present work we considered a nominal 1 mm thick, cold rolled steel (DC01). Mechanical properties parallel, perpendicular and 45° to the rolling direction are given in *Table 1*. The plane strain tensile tests were performed by a geometry shown in *Figure 1* (Wagoner, 1980). It was considered as the basic shape, on which subsequent improvements are proposed in this paper.

Where: A80 is the total engineering strain, A80_ave is the average total engineering strain, r is the r-value, $\bar{r} = \frac{(r0+r90+2\,.r45)}{4}$ is the normal anisotropy, $\Delta r = \frac{r_0+r_{90}}{2} - r_{45}$ is the planar anisotropy, Rp0.2 is the yield strength, Rp0.2_ave is the average yield strength, Rm is the tensile strength and Rm_avr is the average tensile strength.

Table 1

Data for the yield and strength parameters of DC01 material

Orientation angle	0°	45°	90°
A80 (%)	40.0	36.0	39.0
A80_ave (%)	38.0		
r	2.35	1.55	2.52
$\bar{\mathbf{r}}$	1.99		
Δr	0.88		
Rp0,2 (N/mm^2)	199	206	198
Rp0,2_ave (N/mm^2)	201		
Rm (N/mm^2)	306	322	298
Rm_ave (N/mm^2)	309		

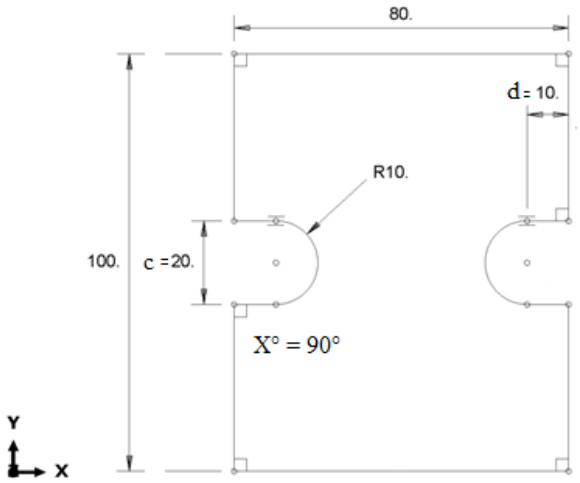

Figure 1. *Sample geometry, used in the plane strain tensile test simulation (units in mm)*

3. FINITE ELEMENT MODELLING

The code used for simulation is Abaqus 2021, with Hill yield criterion developed by Hill in 1948 [(1), written in terms of the Lankford coefficients (r)]. In order to calculate the plastic stress-strain behaviour of the investigated materials, the Swift non-linear isotropic hardening model, shown in equation (2), was used with our measured data shown in *Table 2*.

All specimens have a 30 mm griping area length on both sides and 0.8 mm mesh size of a three-dimensional eight-node brick element with six integration points is used. The boundary and loading conditions are applied in a manner that is as similar to the real tensile test experiment as possible. The lower grip of the specimen was kept fixed in all directions but free in the direction of the applied load. The sliding between grips and specimen is neglected. The maximum major and minor strain values are extracted in the strain hardening region before the local cross-sectional area becomes significantly smaller than the average (necking region). The data gathered from nine points in the middle area of all samples were, as shown in *Figure 2*.

$$\Phi(\sigma) = \frac{r_{TD}(r_{RD}+1)\sigma_{11}^2 + r_{RD}(r_{TD}+1)\sigma_{22}^2 - 2r_{RD}r_{TD}\sigma_{11}\sigma_{22} + (r_{RD}+r_{TD})(2r_{45^\circ}+1)\sigma_{11}^2}{r_{TD}(r_{RD}+1)} - \bar{\sigma} = 0 \qquad (1)$$

$$\bar{\sigma} = K(\varphi_0 + \bar{\varphi})^n \qquad (2)$$

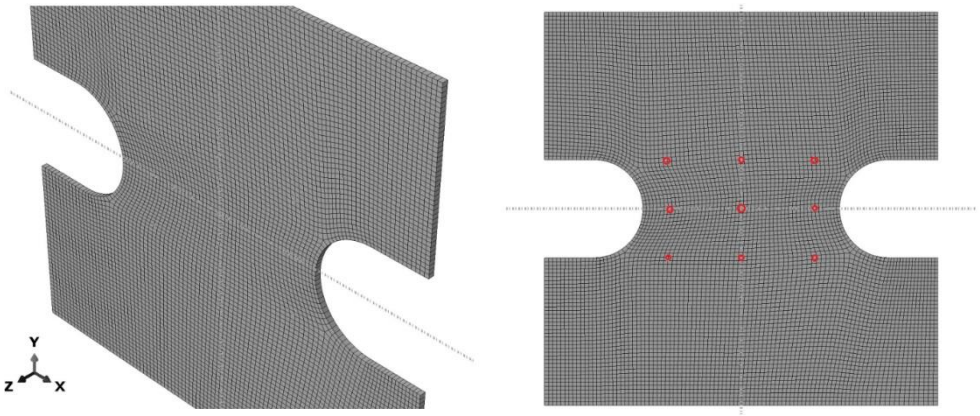

Figure 2. *Mesh and data points of the standard geometry*

Table 2

Swift equation data for the used materials

Material	**Swift equation**		
	K [MPa]	**φ0 [–]**	**n [–]**
DC01	578	0.0173	0.22

In (1) and (2), $\bar{\sigma}$, $\bar{\varphi}$, are respectively the current yield stress and anisotropic equivalent plastic strain, TD refers to the transverse and RD to the rolling direction. Hardening is defined by the material parameters K, n and φ_0 and those are nominated in *Table 2.*

4. TESTING METHODS

To study the effect of various notch geometries (X, d, C) on the strain field distributions, the L27 (313) Taguchi standard orthogonal array is adopted as the testing method. The factors and their levels in the present study are presented in Table 3.

Table 3

Orthogonal array for responses and their levels

X (degree)	**d (mm)**	**c (mm)**	**PSSI min**	**HI min**
		15	–0.1203	0.4168
		20	–0.0974	0.3175
	2.5	25	–0.0959	0.2898
		15	–0.0914	0.3811
		20	–0,0847	0,2304
	5	25	–0,0838	0,2057
		15	–0,0929	0,3350
		20	–0,0719	0,2168
90	10	25	–0,0435	0,1602

X (degree)	d (mm)	c (mm)	PSSI min	HI min
		15	–0.1329	0.7350
		20	–0.1018	0.3715
	2.5	25	–0.0996	0.2930
		15	–0.1133	0.4453
		20	–0.1018	0.3715
	5	25	–0.0999	0.2630
		15	–0.0936	0.3570
		20	–0.0899	0.2476
95	10	25	–0.0633	0.1914
		15	–0.2435	0.9350
		20	–0.2235	0.7239
	2.5	25	–0.1986	0.4930
		15	–0.2345	0.7435
		20	–0.2105	0.4684
	5	25	–0.1850	0.3326
		15	–0.1532	0.5138
		20	–0.1403	0.5021
100	10	25	–0.0995	0.2923

For characterizing the strain state, we used the following equations:

Plane strain state index (PSSI): the closer the average minor strain (ε2) to zero, the better it is.

$$PSSI = A_{\varepsilon 2} = \frac{\sum_{i=1}^{n} \varepsilon_2}{n} \quad (n = 1 \dots 9) \tag{3}$$

Homogeneity index (HI) (equivalent with standard deviation): the smaller the HI, the better is the result.

$$HI = \sqrt{\frac{\sum_{i=1}^{n} (\varepsilon_1^n - A_{\varepsilon 1})^2}{n}} \quad (n = 1 \dots 9) \tag{4}$$

5. MODELLING BY RESPONSE SURFACE METHODOLOGY

The relationship between the factors and the output parameters was modelled by quadratic regression. The regression equations obtained are given below by (5), and (6) with coefficients of determination R2 of 96.34%, and 94.38%, respectively. These regression models help predict the response parameters with respect to the input control parameters.

$$\textbf{PSSI min} = -11.95 + 0.27\,X - 0.0187\,C + 0.000814\,X\,d + 0.000222\,X\,C + 0.000177\,d\,C - 0.001507\,X^2 + 0.000414\,d^2 - 0.000002\,C^2 \tag{5}$$

$$\textbf{HI min} = 14.45 - 0.346\,X + 0.0792\,d + 0.1089\,C - 0.002150\,X\,d - 0.001991\,X\,C + 0.001908\,d\,C + 0.002238\,X^2 + 0.00487\,d^2 + 0.001076\,C^2 \tag{6}$$

6. MODELLING BY ARTIFICIAL NEURAL NETWORK

The purpose of applying this artificial intelligent (AI)-based method is because of their ability to model the highly nonlinear processes. A neural network consists of a directed weighted graph whose nodes symbolize neurons; these neurons have an activation function to influence other network neurons (Chabbi et al., 2017). We used JMP Pro predictive analytics software, it provides advanced algorithms for building, assessing and managing predictive models.

The test design consists of 27 tests; among them, 18 tests are used for learning the network and 9 are arbitrarily chosen for validating the network. The neural network learning is made by backpropagation algorithm, which is based on the gradient-descent method.

Several network structures were tested for both PSSI and HI. According to the correlation coefficient R2 and the root-mean-square error (RMSE) for both learning and validation sets, the adopted structures are shown in *Table 4*.

Table 4
ANN structures of PSSI and HI

Response	Nodes number Input-hidden-output	Learning		Validation	
		R2	RMSE	R2	RMSE
PSSI	3-4-1	0.9964	0.0029	0.9805	0.0087
HI	3-6-1	0.9824	0.0026	0.9723	0.0048

The comparison between RSM and ANN showed that, the values of R2 of the ANN models are better. That's proves the robustness and the reliability of the ANN method. The ANN models are expressed as follows:

$$\textbf{PSSI min} = -0.1525 - 0.0002\ \mathrm{H1} + 0.0231\ \mathrm{H2} + 0.0578\ \mathrm{H3} + 0.0253\ \mathrm{H4} \tag{7}$$

where

$$H1 = \tanh\left(5\,(0.577\,X - 0.4556\,d - 0.3363\,C - 44.7319)\right);$$
$$H2 = \tanh\left(5\,(-0.06\,X - 0.4034\,d + 0.5728\,C - 3.3808)\right);$$
$$H3 = \tanh\left(5\,(-1.4098\,X - 0.438\,d + 0.1278\,C + 134.5717)\right);$$
$$H4 = \tanh\left(5\,(-0.2553\,X + 0.9046\,d - 0.2511\,C + 23.7027)\right);$$

$$\textbf{HI min} = 1.6204 - 2.8529\,H1 + 2.7680\,H2 + 2.0635\,H3 - 0.3214\,H4 - 0.5363\,H5 - 0.7615\,H6 \tag{8}$$

where

$$H1 = \tanh\left(5\,(-0.1081\,X + 0.0981\,d + 0.0387\,C + 9.3979)\right);$$
$$H2 = \tanh\left(5\,(-0.0633\,X + 0.2012\,d + 0.0607\,C + 3.4180)\right);$$
$$H3 = \tanh\left(5\,(-0.0638\,X - 0.1956\,d - 0.0110\,C + 7.1946)\right);$$

$$H4 = \tanh\left(5\,(0.0135\,X + 0.0541\,d + 0.0015\,C - 1.6519)\right);$$
$$H5 = \tanh\left(5\,(-0.011\,X - 0.0291\,d + 0.0097\,C + 1.1673)\right);$$
$$H6 = \tanh\left(5\,(-0.0662\,X - 0.0761\,d + 0.1098\,C + 4.7903)\right);$$

where HI are the terms represent the output of the hidden layer.

The previous models can predict plane strain state index (PSSI) and homogeneity index (HI) in the range of selected sample geometries. *Figure 3* illustrate the differences between the modelled and predicted responses of HI and PSSI. These figures indicate that the models can represent the system under the given studied domain.

Figure 3. *Comparison of the modelled and predicted ANN method values for PSSI and HI*

7. SUMMARY

In our study, the prediction of strain distribution during the plane strain tensile test using the response surface methodology (RSM) and the artificial neural network (ANN) methods is carried out. The comparison between the two modelling methods showed that ANN is better with the values of R2. The comparison of the measured and predicted ANN method values for PSSI and HI figures indicates that the models can represent the system under the given studied domain.

REFERENCES

[1] An, Y. G., Vegter, H. & Elliott, L. (2004). A novel and simple method for the measurement of plane strain work hardening. *Journal of Materials Processing Technology*, 155–156, 1616–1622. https://doi.org/10.1016/j.jmatprotec.2004.04.344

[2] Chabbi, A., Yallese, M. A., Nouioua, M., Meddour, I., Mabrouki, T. & Girardin, F. (2017). Modeling and optimization of turning process parameters during the cutting of polymer (POM C) based on RSM, ANN, and DF methods. *The International Journal of Advanced Manufacturing Technology*, 91, 2267–2290, https://doi.org/10.1007/s00170-016-9858-8.

[3] Flores, P., Tuninetti, V., Gilles, G., Gonry, P., Duchêne, L., & Habraken, A. M. (2010). Accurate stress computation in plane strain tensile tests for sheet metal using experimental data. *Journal of Materials Processing Technology*, 210 (13), 1772–1779, https://doi.org/10.1016/j.jmatprotec.2010.06.008.

[4] Goodwin, G. & Gorton, M. (1968). Application of strain analysis to sheet metal form-ing problems in the press shop. *SAE Technical Paper*.

[5] International Organization for Standardization. (2008). ISO/DIS 12004-2: 2008. Metallic Materials–Sheet and Strip. *Determination of Forming Limit Curves–Part 2: Deformination of Forming limit Curves in the Laboratory*. International Organization for Standardization.

[6] Keeler, S. & Backofen, W. (1964). Plastic instability in sheet stretched over rigid punches. *ASM Transactions Quarterly*, 11, 25–48.

[7] Kuwabara, T. (2007). Advances in experiments on metal sheets and tubes in support of constitutive modeling and forming simulations. *International Journal of Plasticity*, 23 (3), 385–419. doi:https://doi.org/10.1016/j.ijplas.2006.06.003

[8] Marciniak, Z. & Kuczyński, K. (1967). Limit strains in the processes of stretch-forming sheet metal. International journal of mechanical sciences 9.9. *International Journal of Mechanical Sciences*, 9 (9), 609–620. doi:https://doi.org/10.1016/0020-7403(67)90066-5

[9] Wagoner, R. H. (1980). Measurement and analysis of plane-strain work hardening. *Metallurgical Transactions A*, 11 (1), 165–175. doi:https://doi.org/10.1007/BF02700453